PAPER

Check for updates

Biodiesel production from soybean oils by a novel nano-magnetic solid base catalyst (K/ZrO$_2$/γ-Fe$_2$O$_3$)

Kang Liu,[ab] Rui Wang [iD] *[a] and Meiqing Yu[ab]

Biodiesel is emerging as a green alternative source to fossil fuels due to its clean and renewable advantages. In this study, a nano-solid base catalyst (K/ZrO$_2$/γ-Fe$_2$O$_3$) with weak magnetism was successfully synthesized and investigated for transesterification of soybean oil to produce biodiesel. The obtained catalyst was fully characterized by X-ray diffraction (XRD), Brunauer–Emmett–Teller (BET), transmission electron microscopy (TEM), vibrating sample magnetometer (VSM), thermogravimetry/differential scanning calorimetry device (TG/DSC), and scanning electron microscopy-energy dispersive X-ray (SEM-EDX) analysis. Results showed that the nano-magnetic catalyst had granular nano-structures with particle sizes of 15–25 nm. The optimum conditions for transesterification were shown to be as follows: catalyst added amount of 5 wt%; methanol/oil molar ratio of 10 : 1; reaction time of 3.0 h, and reaction temperature of 65 °C, and the yield of biodiesel could reach above 93.6 wt%. The reusability of the magnetic catalyst demonstrated that the magnetic catalyst was ferromagnetic and still maintained high catalytic activity after six times' reuse. The formed core–shell was hard to separate even after stirring in liquid phase reactions, which was favorable for use in biodiesel production. The developed nano-magnetic catalyst shows a potential application for biodiesel production in a green manner.

1. Introduction

The growing demand for energy around the world has aroused great attention to the exploration of new fuels and energy.[1,2] Nowadays, biodiesel is emerging as an alternative diesel fuel for fossil fuels.[3,4] Biodiesel, which can be synthesized by the transesterification of waste oils or animal fats with a short-chain alcohol, is considered a new renewable energy source.[5,6] In previous studies, biodiesel has been confirmed to be better than diesel fuel with a series of advantages, such as sulfur content, aromatic content, and cetane number.[7,8] Besides, compared to normal diesel, biodiesel is non-toxic and bio-degradable.[9] Thus, the emission of greenhouse gases can be greatly reduced.[10,11]

Generally, transesterification reactions can be catalyzed by using a suitable catalyst, such as an inorganic base, inorganic acid or enzyme with high reactivity.[12,13] Though homogeneous base catalysts have been confirmed to provide much faster reaction rates than heterogeneous catalysts, they also present many defects in biodiesel production, such as damaging the equipment, difficulty of product separation, and reclamation difficulty.[14,15] To overcome these disadvantages of

homogeneous catalysts, nano-magnetic catalysts were considered as ideal replacements for catalytic reactions.[16,17]

The previous studies indicated that nano-magnetic catalysts with high ratio surface area and high surface energy may be a better choice for biodiesel production.[18–20] Meanwhile, compared with the conventional heterogeneous catalysts, the nano-magnetic catalysts would be easily separated and reused by external magnetic field after the transesterification reaction.[21,22] Zhang *et al.*[23] developed a magnetic catalyst (Na$_2$SiO$_3$@Fe$_3$O$_4$/C) for biodiesel production from oils under ultrasonic (US) irradiation. The magnetic catalyst could be easily magnetically separated for five cycles with 94.9 wt% recovery rate. Xue *et al.*[24] prepared a novel magnetic catalyst (CaFe$_2$O$_4$–Ca$_2$Fe$_2$O$_5$) by co-precipitation and calcination. The catalysts could be recycled three times with above 78.2 wt% biodiesel yield. These reports indicated that the magnetic solid base catalyst is an efficient and green catalyst for the industrial production of biodiesel. Therefore, to develop the new magnetic catalyst not only provides a new choice for the biodiesel production, but also provides a new technology for the rapid recovery and separation of the catalysts.

Herein, a magnetic catalyst with nano-structure, named as K/ZrO$_2$/γ-Fe$_2$O$_3$ was successfully prepared by sol–gel method. The obtained magnetic catalyst was applied as a catalyst in the transesterification reaction with methanol as reaction reagent. The structure and properties of the magnetic catalyst was fully characterized by X-ray diffraction (XRD),

[a]*Shenzhen Research Institute of Shandong University, Shenzhen 518057, Guangdong, China. E-mail: wangrui@sdu.edu.cn*

[b]*School of Environmental Science & Engineering, Shandong University, Jinan 250199, China*

Brunauer–Emmette–Teller (BET), transmission electron microscope (TEM), vibrating sample magnetometer (VSM), thermogravimetry/differential scanning calorimetry device (TG/DSC). The preparation conditions and the optimal parameters of transesterification were also studied. The results demonstrated that the magnetic particles were fully encapsulated in the ZrO_2 particles, which was beneficial to the separation and recycle. The conjunction of ZrO_2 and Fe_2O_3 not only presented strong psychic magnetism of catalysts, but also significantly prevented the magnetic particles loss.

2. Materials and methods

2.1. Materials and reagents

Soybean oil was purchased from supermarket (Jinan, China). Ammonia solution (25 wt%), methanol, potassium hydroxide (KOH), zirconium oxychloride ($ZrOCl_2 \cdot 8H_2O$), ferrous chloride tetrahydrate ($FeCl_2 \cdot 4H_2O$) and six hydrated ferric chloride ($FeCl_3 \cdot 6H_2O$) were purchased from Sinopharm (Shanghai, China). Methyl linoleate, methyl palmitate, methyl oleate, methyl stearate, methyl linolenate, and methyl heptadecanoate, used as standard materials, were purchased from J&K (Beijing, China). Deionized water was used for preparation and dilution of chemical solutions.

2.2. Preparation of nano-magnetic catalyst

The $FeCl_2 \cdot 4H_2O$ and $FeCl_3 \cdot 6H_2O$ with a mole proportion of 1 : 2 were synchronously dissolved in the deionized water. $ZrOCl_2 \cdot 8H_2O$ were then dropped into mixed solution with constantly stirring. Ammonia of 25 wt% was then added into the above solution in a water bath with the heating temperate of 25 °C. The gel–sol ($Zr(OH)_4$–$Fe(OH)_3$) produced by the chemical reaction can be obtained after filtration, separation and washing treatment. After drying the free water at 105 °C, the gel–sol $KOH/(Zr(OH)_4$–$Fe(OH)_3)$ was prepared by impregnation of the zirconium hydroxide with an aqueous solution of KOH. The impregnated precursor was calcined in a muffle furnace with different temperature. Finally, the obtained solid powder was viewed as nano-magnetic catalyst solid base catalyst $K/ZrO_2/\gamma$-Fe_2O_3 (Fig. 1).
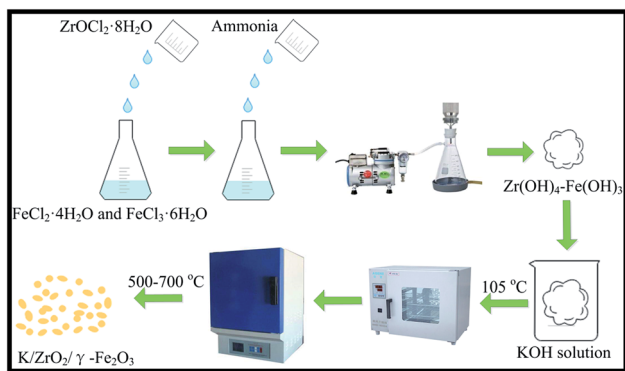

Fig. 1 Synthesis diagram of the nano-magnetic catalyst $K/ZrO_2/\gamma$-Fe_2O_3.

2.3. Transesterification of soybean oil with methanol

At the beginning of the experiment, a certain proportion of soybean oil, methanol, and the obtained nano-magnetic catalyst $K/ZrO_2/\gamma$-Fe_2O_3 were together added into a 100 ml neck flask with vigorous stirring. The water bath temperature for the transesterification reaction was controlled between 50 and 70 °C. After transesterification reaction in a set reaction time, the nano-magnetic catalyst could be recovered by a permanent magnet. The reaction sample after transesterification reaction became biphasic. After split-phase, the upper phase containing the biodiesel was revolved to remove the superfluous methanol. And the purified sample was directly analyzed the yield of biodiesel by using a gas chromatography.

2.4. Analysis and characterization

To detect the biodiesel yield, methyl heptadecanoate was employed as an internal standard. And normal hexane was used as diluted solvent. The yield of biodiesel samples after transesterification reaction was analyzed by a SP-6800 gas chromatograph equipped with a flame ionization detector and a capillary column AT. FFAP (30 m × Φ 0.32 mm × 0.33 μm). The yield of biodiesel was calculated by the following equation:

$$\text{yield}_{FAME} = \frac{\sum f_{ester} A_{ester}}{A_{internal}} \times \frac{m_{internal}}{m_{esters}} \times 100\% \qquad (1)$$

following the above formula, A_{ester} is the peak area of methyl esters, $A_{internal}$ is the peak area of internal standard, $m_{internal}$ is the mass of internal standard, m_{esters} is the mass of fatty acid methyl esters and f_{ester} is the correction factor of fatty acid methyl esters.

The specific surface area was calculated by Brunauer–Emmett–Teller (BET) method from the linear part of the nitrogen adsorption isotherms. Total pore volume (V_{tot}) was given at $p/p^0 = 0.998$. The mesopores volume and pore size distribution were calculated according to the Barrett–Joyner–Halenda (BJH) method from the desorption branch of isotherm. The nitrogen adsorption and desorption isotherms were measured at −196 °C using NDVA2000e analytical system made by Qunta chrome Corporation (USA). Before the measurement all samples were degassed at 120 °C for 12 h under reduced pressure (<1 torr) prior to sorption measurements. X-ray diffraction (XRD) patterns of selected samples were recorded by the reflection scan with nickel-filtered Cu Ka radiation (D8, Bruker-AXS, Germany). The X-ray generator was run at 40 kV and 60 mA. All the XRD measurements were performed at 2θ values between 10 and 80°. Thermal decomposition was evaluated by thermogravimetric analysis (TGA) and differential scanning calorimetry (DSC) was carried out on a SDT Q600 Universal V4.1D TA instrument operating under a flow of N_2 at a 10 °C min^{-1} heating rate up to 700 °C. Magnetization curves were measured on a vibrating sample magnetometer (LDJ9500, VSM, the United States) with a magnetic field of 10 000 Oe. Metal contents of the biodiesel samples were determined by inductively coupled plasma-optical emission spectrometer (ICP-OES, OPTIMA 8300, PerkinElmer, USA) and inductively coupled plasma mass spectrometry (ICP-MS, NexION 350, PerkinElmer,

USA), respectively, after the HNO₃–HCl–HF digestion. The morphological property of the catalyst was examined by a scanning electron microscope with energy dispersive X-ray analysis (SEM-EDX, Hitachi S-3000N, Japan).

3. Results and discussion

3.1. Effect of the preparation conditions on biodiesel yield

Various preparation conditions, such as KOH loading amount and calcination temperature of magnetic catalyst was evaluated in the transesterification of soybean oil with methanol. A series of K/ZrO$_2$/γ-Fe$_2$O$_3$ catalysts with KOH loaded ranging from 10 to 35 wt% were prepared and calcined at 600 °C in air for 4 h. The biodiesel yield was improved from 41.4 wt% to 90.4 wt% when the KOH loading increased from 10 wt% to 30 wt% (Fig. 2a). It shows that the increasing of KOH loading amount was favor for the increase of the active sites of catalyst surface. When the KOH loading amount was beyond 30 wt%, the activity of catalyst was decreased significantly. Therefore, the optimum loading amount of KOH was 30 wt%. In the preparation process of catalyst, calcination treatment of catalyst at high temperature was favorable for the interaction between support and active ingredient, which generated new active sites for the catalyst. With the increase of calcination temperature, the biodiesel yield significantly increased as the calcinations temperature rose from 500 °C to 600 °C. And the yield of biodiesel reached the highest 90.4 wt% (Fig. 2b). However, the yield decreased slightly after the temperature exceeded 600 °C. Therefore, the best calcination temperature for catalyst preparation was 600 °C.

Previous research had documented that, ZrO$_2$ can be regarded as a best support for the rich vacancies on the surface which the cations were easy to be inserted in.[25–27] The crystallization of Zr(OH)$_4$ created a considerable number of vacancies on the surface of ZrO$_2$ during heating treatment. The molten KOH released K$^+$ into the vacancies and the K$^+$ possibly occupy the position of octa-coordinated Zr^{4+} to form K–O–Zr solid solution, forming strong basic and super basic sites. The main contribution to the transesterification is the new-formed active sites
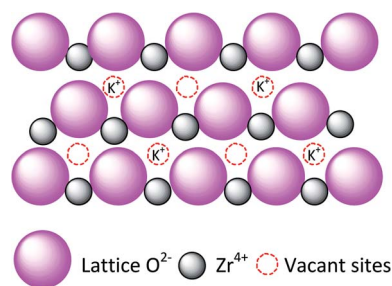

Fig. 3 Diagram of the major mechanism of active sites for transesterification.

of KO$_x$ species and K–O–Zr groups (Fig. 3). Thus, a high temperature was favorable for the production of oxygen vacancies. But the high temperature also caused the agglomeration of catalyst and the decrease of specific surface area, which directly led to an inferior catalytic activity.

3.2. Catalyst characterization

3.2.1. BET. Table 1 showed that the catalyst possessed a surface area of 20.08 m^2 g^{-1}, pore volume of 0.051 m^3 g^{-1} and an average pore diameter of 10.146 nm. The BET isotherm of the catalyst was of type IV. The H$_3$ hysteresis loop at relative pressure 0.6–0.998 indicated that the magnetic catalyst possessed the characteristics of mesoporous materials (Fig. 4)

3.2.2. SEM-EDX and TEM. It can be seen from Fig. 5 that the zirconia particles exhibited tetragonal shape. These zirconia particles were distributed homogeneously and evenly. According to speculation, iron oxide nanoparticles were wrapped by the zirconia particles. The coated structure of nano-magnetic catalyst was characterized by TEM analysis. Fig. 6a and b shows that the black Fe$_2$O$_3$ was coated by Zr(OH)$_4$ with the amorphous form in precursor. The typical coated structure of K/ZrO$_2$/γ-Fe$_2$O$_3$ can be clearly observed, indicating the successful coating of ZrO$_2$ on Fe$_2$O$_3$ by sol–gel method (Fig. 6c). The diameter of K/ZrO$_2$/γ-Fe$_2$O$_3$ was approximately 20 nm.
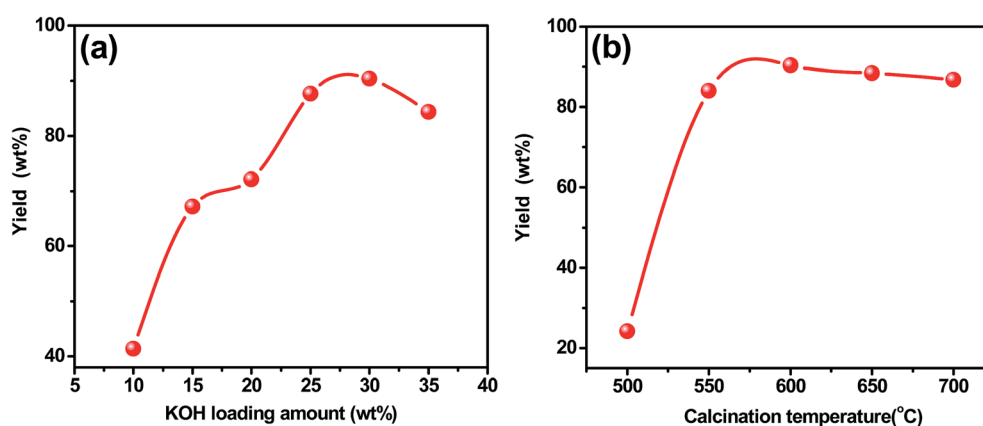

Fig. 2 Effects of (a) KOH loading amount; (b) calcination temperature (transesterification conditions: reaction temperature: 65 °C; methanol/oil: 8 : 1; catalyst amount: 4 wt%; reaction time: 3 h).

Table 1 Physicochemical properties of magnetic catalyst[a]

Sample	Molar ratio Fe : Zr	S_{BET} ($m^2\ g^{-1}$)	D_{av} (nm)	V_{total} ($cm^3\ g^{-1}$)	V_{mic} ($cm^3\ g^{-1}$)
ZFK	1 : 15	20.08	10.146	0.051	0.0081

[a] S_{BET}, D_{av}, V_{total}, and V_{mic} denote BET surface area, total pore volume, micro porous total pore volume and average pore diameter, respectively. ZFK represents the precursor with 30 wt% KOH loading amount after calcining at 600 °C for 4 h.
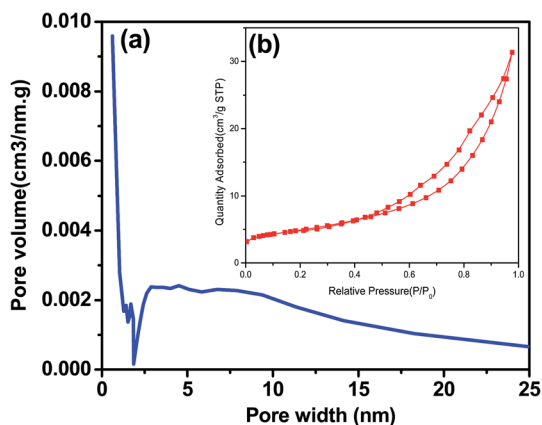
Fig. 4 (a) Pore size distribution curves. (b) Nitrogen adsorption–desorption isotherm.

3.2.3. XRD. Fig. 7 demonstrates the XRD patterns of precursor with different calcination temperature. The XRD pattern in the top right-hand corner presented that the precursor appeared amorphous diffraction peak at 10°–30°. The tetragonal form ($2\theta = 30.28°$, $50.48°$, and $60.28°$) appeared after calculation at 600 °C, indicating that the $Zr(OH)_4$ was converted to tetragonal crystal (t-ZrO_2). Subsequently, the monoclinic baddeleyite phase ($2\theta = 28.2°$) appeared after calculation at 700 °C, indicating that partial tetragonal crystal in ZrO_2 was converted to monoclinic baddeleyite (m-ZrO_2).

3.2.4. TG-DSC. The TG-DSC curve presented the weight loss of precursor during heating treatment (Fig. 8). The TG peak around 100 °C was assigned to the loss of physical adsorbed H_2O, while the other one around 100–500 °C could be attributed to the removal of hydroxyl groups in $Zr(OH)_4$. The TG-DSC curve of precursor exhibited an exothermic weight loss around 613.23 °C, indicating the decomposition of KOH. The results suggested that the best calcination temperature for catalyst preparation was 600 °C, which was in accordance with the result in Section 3.1.

3.2.5. VSM. Fig. 9 demonstrates that all the magnetic catalyst samples, including the precursor, recovery catalyst and the catalysts calcined at different temperature, had the ferro-magnetic behavior characteristic and show superparamagnetism (all curves go through the zero point). The saturation magnetization of precursor was the highest 23.3 emu g^{-1} due to the existence of Fe_3O_4. The magnetization of catalyst calcined at 500 °C (9.91 emu g^{-1}) was weaker than the precursor, because the Fe_3O_4 was oxidized to γ-Fe_2O_3 during the calcination process which led to the decrease of magnetization.[28] But when the catalyst was calcined at 600 °C, the saturation magnetization (15.4 emu g^{-1}) of magnetic catalyst increased markedly. Combined with the result of XRD test, it could be concluded that the molecular layer of zirconia crystal tended to grow thin with the removal of hydroxyl groups on the surface of $Zr(OH)_4$, resulting in the increase of mass ratio of γ-Fe_2O_3. Part of iron oxide nano-particles, originally coated by $Zr(OH)_4$, exposed in the

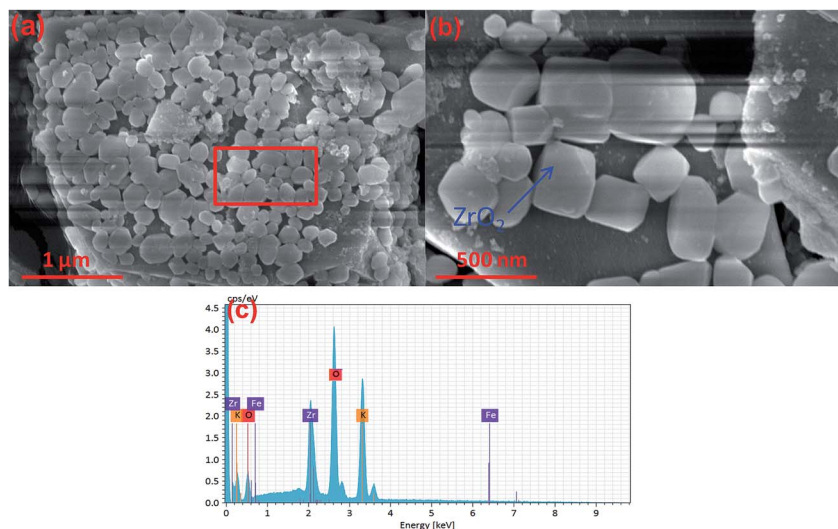Fig. 5 (a, b) SEM images and (c) EDX of the nano-magnetic catalyst K/ZrO_2/γ-Fe_2O_3.
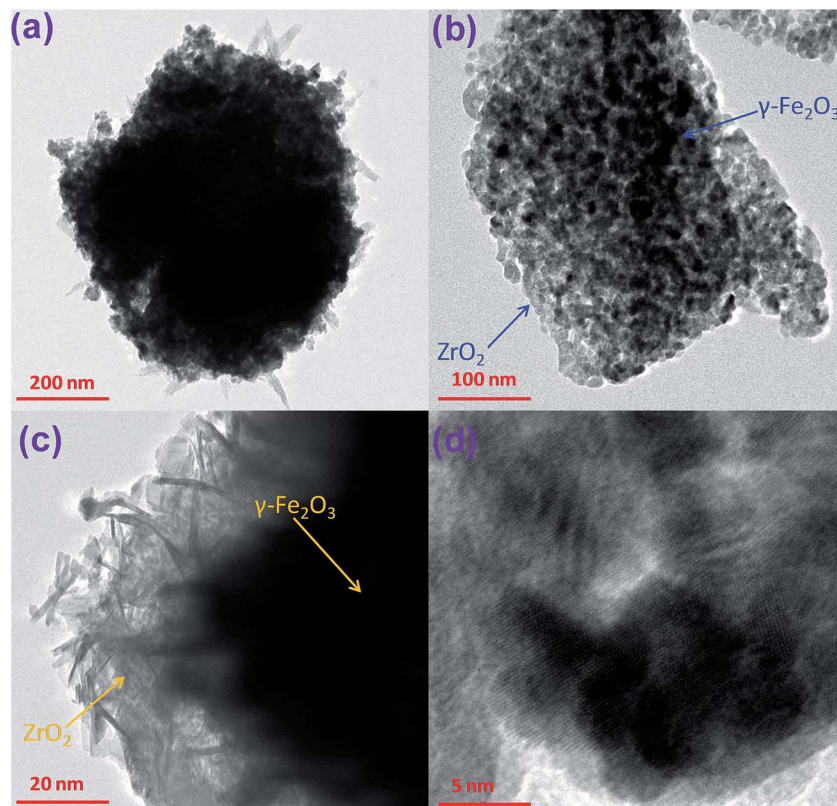
Fig. 6 TEM images of the nano-magnetic catalyst K/ZrO$_2$/γ-Fe$_2$O$_3$ at different scale.

environment, which led to the increase of the saturation magnetization. This result revealed that the coated layers significantly affected the magnetic properties of the catalysts. In comparison, the saturation magnetization of the magnetic catalyst calcined at 700 °C was only 11.03 emu g^{-1}, indicating that the γ-Fe$_2$O$_3$, coated by ZrO$_2$ nanoparticles, was converted to α-Fe$_2$O$_3$ completely.[29]

3.3. Optimization of transesterification catalyzed by magnetic catalyst

Fig. 10a indicates that the reaction rate was slow at low temperatures and the biodiesel yield was only 67.8 wt% at 50 °C

after 3 h of reaction. The biodiesel yield increased with the increase of reaction temperature to nearly 90.4 wt% at 65 °C, but at higher temperatures ($T > 65$ °C), the methanol was vaporized and formed a large number of bubbles in the interface, which inhibited the increase of biodiesel yield, then the yield of biodiesel decreased significantly. Thus, the optimum reaction temperature was 65 °C. As presented in Fig. 10b, the biodiesel yield increased from 48.5 wt% to 92.5 wt% as the molar ratio increased from 4 : 1 to 10 : 1 through 3 h of reaction. However, beyond the molar ratio of 10 : 1, the excessively added methanol had no significant effect on the production yield. When the amount of methanol was over 12 : 1, glycerol separation became
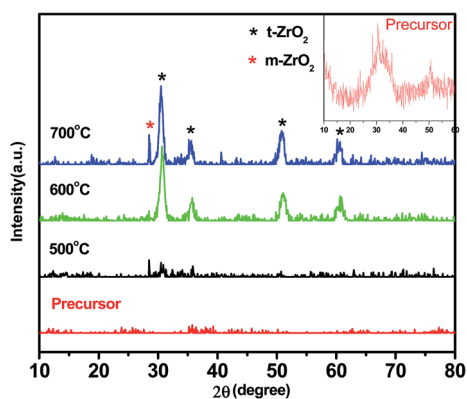

Fig. 7 XRD patterns of the magnetic precursor after calcining at different temperature.
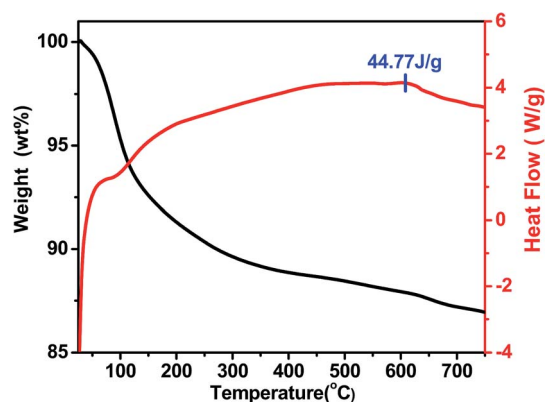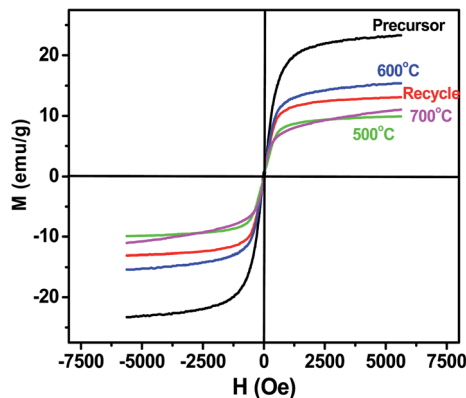

Fig. 8 The TG-DSC of the precursor.

Fig. 9 Hysteresis curve of nano-magnetic catalyst.

more difficult, thus decreasing the biodiesel yield. Based on this, the optimum molar ratio of methanol to oil was 10 : 1. The mass ratio of magnetic catalyst to soybean oil was varied within the range of 2–6 wt% (Fig. 10c). The biodiesel yield was increased with increasing catalyst and the maximum biodiesel yield was obtained by adding 5.0 wt% magnetic catalyst, which reached 93.6 wt% at 3 h. The results indicated that with more catalyst addition, there was a faster rate at which reaction equilibrium was reached because of the increase in the total number of available active catalytic sites for the reaction. However, with further increase the catalyst amount, the bio-diesel yield decreased, which was possibly due to the saponifi-cation. And only 77 wt% yield was obtained when the mass ratio was 6.0 wt%. Therefore, the optimum catalyst amount was

proved to be 5.0 wt%. Fig. 10d reveals that the trans-esterification reaction was strongly dependent on reaction time. At the beginning (<1.5 h), the reaction was slow due to the mixing and the dispersion of methanol into oil, and the bio-diesel yield was increased in the reaction time range between 1.5 h and 3.5 h. Moreover, excess reaction time led to a bit reduction in the product yield due to the backward reaction transesterification, resulting in a loss of esters as well as causing more fatty acids to form soaps. Thus, the optimum reaction time was 3.0 h. In summary, the optimum conditions for transesterification were shown as follows: catalyst/oil molar ratio of 5 wt%; methanol/oil molar ratio of 10 : 1; reaction time of 3.0 h, and reaction temperature of 65 °C, and the yield of biodiesel could reach above 93.6 wt%. Compared with other magnetic catalysts ($CaFe_2O_4$–$Ca_2Fe_2O_5$ 85.4 wt% (ref. 24) and $CaO/CoFe_2O_4$ 87.4 wt% (ref. 30)), the synthesized magnetic catalysts $K/ZrO_2/\gamma$-Fe_2O_3 exhibited obvious advantages in the production of biodiesel.

3.4. Reusability of magnetic catalyst

The reusability of the magnetic catalyst is shown in Fig. 11. After reusing six times at 65 °C, the yield of biodiesel was about 74.1 wt% (Fig. 11a). Accordingly, the recovery rate of the catalyst also showed an obvious downward trend. This indicated that the catalyst was inevitably lost in the use and recovery process of the magnetic catalyst. Fig. 11b shows that the Zr, Fe and Zr elements from the $K/ZrO_2/\gamma$-Fe_2O_3 catalyst were detected in the prepared biodiesel. The cumulative content showed an upward trend with the increase of the used number of the catalyst. Combined with the SEM analysis of Fig. 11c and d, it was found
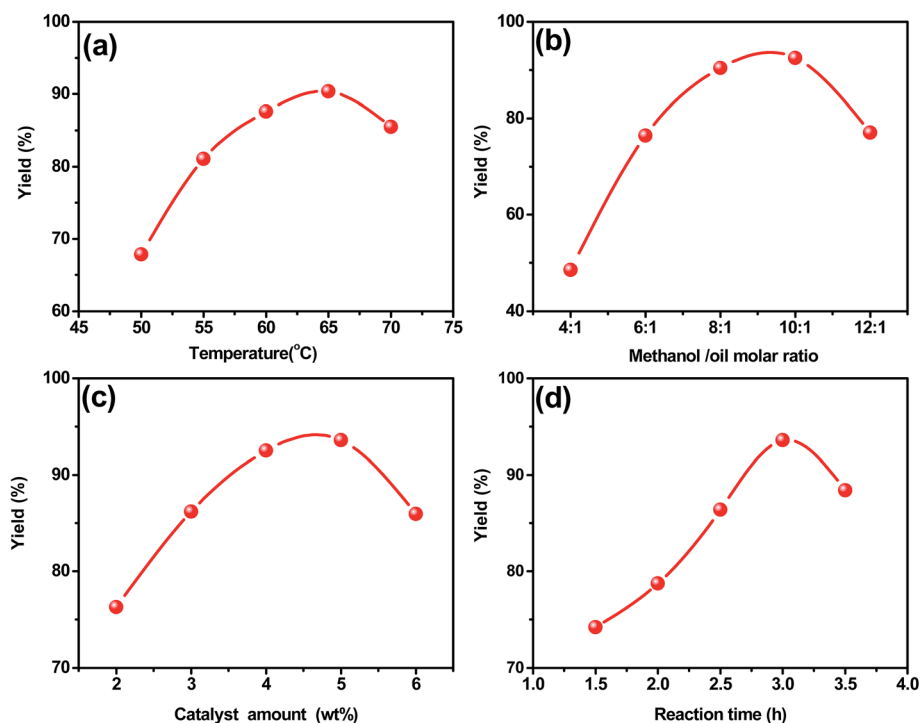

Fig. 10 Effects of (a) reaction temperature (b) methanol/oil (c) catalyst amount (d) reaction time on biodiesel yield.
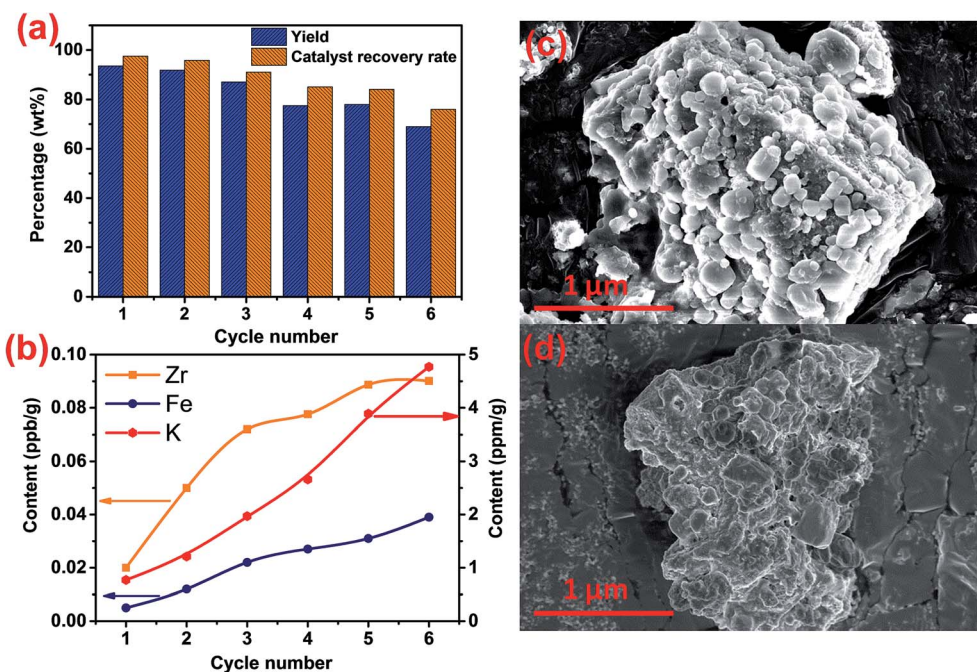
Fig. 11   (a) Reusability of the magnetic catalyst K/ZrO$_2$/γ-Fe$_2$O$_3$ (b) accumulation of the Zr, Fe and K elements in the prepared biodiesel (c) SEM result of the initial catalyst K/ZrO$_2$/γ-Fe$_2$O$_3$ (d) SEM result of the catalyst K/ZrO$_2$/γ-Fe$_2$O$_3$ after six times of use (transesterification conditions: reaction temperature: 65 °C; methanol/oil: 10 : 1; catalyst amount: 5 wt%; reaction time: 3 h).

that the zirconia particles fell off from the surface of the magnetic catalyst after six times of use. Besides, the surface of the magnetic catalyst presented obvious sintering phenomenon due to multiple calcination. Therefore, the decline of yield could be considered as the loss of nano-power and alkaline sites in the process of recycling process of the K/ZrO$_2$/γ-Fe$_2$O$_3$ catalyst.

4.   Conclusion

A nano-magnetic solid base catalyst K/ZrO$_2$/γ-Fe$_2$O$_3$ was developed by sol–gel method and characterized by various techniques. The results indicated that the nano-magnetic catalyst had a unique coated structure with an average particle diameter of 20 nm and a ferromagnetic property. Based on the experiments, the optimum conditions for transesterification were shown as follows: catalyst/oil molar ratio of 5 wt%; methanol/oil molar ratio of 10 : 1; reaction time of 3.0 h, and reaction temperature of 65 °C, and the yield of biodiesel could reach above 93.6 wt%. The nano-magnetic catalyst, K/ZrO$_2$/γ-Fe$_2$O$_3$, used in the preparation of biodiesel illustrates a good prospect of development and appears to be a promising candidate in substitution for conventional catalysts due to the high activity and their unique magnetic properties.

Conflicts of interest

There are no conflicts to declare.

Acknowledgements

References

1   Y. Wang, S. De and N. Yan, *Chem. Commun.*, 2016, **52**, 6210–6224.
2   W. Li, Y. Gao, S. Yao, D. Ma and N. Yan, *Green Chem.*, 2015, **17**, 4198–4205.
3   S. K. Hoekman, A. Broch, C. Robbins, E. Ceniceros and M. Natarajan, *Renewable Sustainable Energy Rev.*, 2012, **16**, 143–169.
4   J. Xue, T. E. Grift and A. C. Hansen, *Renewable Sustainable Energy Rev.*, 2011, **15**, 1098–1116.
5   J. Yang, M. Xu, X. Zhang, Q. Hu, M. Sommerfeld and Y. Chen, *Bioresour. Technol.*, 2011, **102**, 159–165.
6   A. E. Atabani, A. S. Silitonga, I. A. Badruddin, T. Mahlia, H. Masjuki and S. Mekhilef, *Renewable Sustainable Energy Rev.*, 2012, **16**, 2070–2093.
7   R. Halim, B. Gladman, M. K. Danquah and P. A. Webley, *Bioresour. Technol.*, 2011, **102**, 178–185.
8   T. Issariyakul and A. K. Dalai, *Renewable Sustainable Energy Rev.*, 2014, **31**, 446–471.
9   R. Halim, M. K. Danquah and P. A. Webley, *Biotechnol. Adv.*, 2012, **30**, 709–732.
10   P. K. Campbell, T. Beer and D. Batten, *Bioresour. Technol.*, 2011, **102**, 50–56.

11 I. Rawat, R. R. Kumar, T. Mutanda and F. Bux, *Appl. Energy*, 2013, **103**, 444–467.

12 Y. Li, Y.-F. Chen, P. Chen, M. Min, W. Zhou, B. Martinez, J. Zhu and R. Ruan, *Bioresour. Technol.*, 2011, **102**, 5138–5144.

13 N. Yusuf, S. K. Kamarudin and Z. Yaakub, *Energy Convers. Manage.*, 2011, **52**, 2741–2751.

14 O. Özener, L. Yüksek, A. T. Ergenç and M. Özkan, *Fuel*, 2014, **115**, 875–883.

15 L. P. Christopher, H. Kumar and V. P. Zambare, *Appl. Energy*, 2014, **119**, 497–520.

16 E. Aransiola, T. Ojumu, O. Oyekola, T. Madzimbamuto and D. Ikhu-Omoregbe, *Biomass Bioenergy*, 2014, **61**, 276–297.

17 A. M. Ashraful, H. Masjuki, M. Kalam, I. R. Fattah, S. Imtenan, S. Shahir and H. Mobarak, *Energy Convers. Manage.*, 2014, **80**, 202–228.

18 B. Liu and Z. Zhang, *ACS Catal.*, 2015, **6**, 326–338.

19 M. Feyzi and L. Norouzi, *Renewable Energy*, 2016, **94**, 579–586.

20 Y. Liu, P. Zhang, M. Fan and P. Jiang, *Fuel*, 2016, **164**, 314–321.

21 T. A. Ngu and Z. Li, *Green Chem.*, 2014, **16**, 1202–1210.

22 K.-L. Chang, Y.-C. Lin, S.-R. Jhang, W. L. Cheng, S.-C. Chen and S.-Y. Mao, *Catalysts*, 2017, **7**, 203.

23 F. Zhang, Z. Fang and Y.-T. Wang, *Fuel*, 2015, **150**, 370–377.

24 B.-j. Xue, J. Luo, F. Zhang and Z. Fang, *Energy*, 2014, **68**, 584–591.

25 S.-F. Yin, B.-Q. Xu, S.-J. Wang and C.-T. Au, *Appl. Catal., A*, 2006, **301**, 202–210.

26 K.-T. Li, C.-K. Wang, I. Wang and C.-M. Wang, *Appl. Catal., A*, 2011, **392**, 180–183.

27 M. Kim, C. DiMaggio, S. Yan, H. Wang, S. O. Salley and K. S. Ng, *Bioresour. Technol.*, 2011, **102**, 2380–2386.

28 M. M. Can, M. Coşkun and T. Fırat, *J. Alloys Compd.*, 2012, **542**, 241–247.

29 M. M. Can, M. Coşkun and T. Fırat, *J. Alloys Compd.*, 2012, **542**, 241–247.

30 P. Zhang, Q. Han, M. Fan and P. Jiang, *Appl. Surf. Sci.*, 2014, **317**, 1125–1130.